International Journal of Thermophysics, Vol. 27, No. 3, May 2006 (© 2006)
DOI: 10.1007/s10765-006-0056-z

Isochoric Heat Capacity of $CO_2 + n$-Decane Mixtures in the Critical Region

N. G. Polikhronidi,[1] R. G. Batyrova,[1] I. M. Abdulagatov,[1–3] and G. V. Stepanov[1]

Received May 27, 2005

The isochoric heat capacity of two binary ($CO_2 + n$-decane) mixtures (0.095 and 0.178 mole fraction of n-decane) have been measured with a high-temperature, high-pressure, nearly constant volume adiabatic calorimeter. Measurements were made at nineteen near-critical liquid and vapor densities between 87 and 658 $kg \cdot m^{-3}$ for the composition of 0.095 mole fraction n-decane and at nine densities between 83 and 458 $kg \cdot m^{-3}$ for the composition of 0.178 mole fraction n-decane. The range of temperatures was 295 to 568 K. These temperature and density ranges include near- and supercritical regions. The measurements were performed in both one- and two-phase regions including the vapor + liquid coexistence curve. The uncertainty of the heat- capacity measurements is estimated to be 2% (coverage factor $k = 2$). The uncertainty in temperature is 15 mK, and that for density measurements is 0.06%. The liquid and vapor one-(C'_{V1}, C''_{V1}) and two-phase (C'_{V2}, C''_{V2}) isochoric heat capacities, temperatures (T_S), and densities (ρ_S) at saturation were measured by using the well-established method of quasi-static thermograms for each filling density. The critical temperatures (T_C), the critical densities (ρ_C), and the critical pressure (P_C) for the $CO_2 + n$-decane mixtures were extracted from the isochoric heat-capacity measurements on the coexistence curve. The observed isochoric heat capacity along the critical isochore of the $CO_2 + n$-decane mixture exhibits a renormalization of the critical behavior of C_{VX} typical for mixtures. The values of the characteristic parameters (K_1, K_2), temperatures (τ_1, τ_2), and the characteristic density differences ($\Delta\bar{\rho}_1, \Delta\bar{\rho}_2$) were estimated for the $CO_2 + n$-decane mixture by using the critical-curve data and the theory of critical phenomena in

[1] Institute of Physics of the Dagestan Scientific Center of the Russian Academy of Sciences, Shamilya Str. 39-A, 367003 Makhachkala, Dagestan, Russia.
[2] Present address: Physical and Chemical Properties Division, National Institute of Standards and Technology, 325 Broadway, Boulder, Colorado 80305, U.S.A.
[3] To whom correspondence should be addressed. E-mail: ilmutdin@boulder.nist.gov

binary mixtures. The ranges of conditions were defined on the T-x plane for the critical isochore and the ρ-x plane for the critical isotherm, for which we observed renormalization of the critical behavior for the isochoric heat capacity.

KEY WORDS: adiabatic calorimeter; carbon dioxide; coexistence curve; critical point; equation of state; isochoric heat capacity; Krichevskii parameter; n-decane; supercritical fluid mixture.

1. INTRODUCTION

Supercritical carbon dioxide is widely used as a solvent in supercritical fluid extractions and a number of separation and reaction processes [1–5]. Carbon dioxide is commonly used in industrial processes such as the processing of petroleum products and enhanced oil recovery. Carbon dioxide is also one of the components of natural gas. Therefore, a knowledge of the thermodynamic properties for CO_2+ hydrocarbon mixtures is relevant for industrial applications such as petroleum and natural gas engineering, and for rational design of chemical reactors and high-pressure extraction and separation equipment. Thermodynamic properties of $CO_2 + n$-decane mixtures are of interest also to the petroleum and natural gas industries, because of the growing interest in the extraction of viscous, low volatility compounds with supercritical CO_2 in tertiary oil recovery and new separation techniques. Near-critical and supercritical carbon dioxide has been used as a miscible flooding agent that promotes miscible displacement of hydrocarbons from underground reservoirs [6–10]. To improve our understanding of the mechanism of the process of miscible displacement of reservoir oils by carbon dioxide injection (oil recovery enhancement) and to control those processes, a better knowledge of model systems would be helpful. Since n-decane is a typical component of petroleum, and since it is available as a high-purity ambient-temperature liquid, it makes a good choice for a model system. Precise measurements are needed to establish the behavior of the thermodynamic properties of $CO_2 + n$-decane mixtures. Although our understanding of the thermodynamic properties of CO_2 and binary (CO_2 + solute) systems at ambient conditions has improved significantly, it is far from sufficient to accurately predict the behavior of (CO_2 + solute) systems for near-critical and supercritical conditions that are currently of great scientific and practical interest. Therefore, to use supercritical CO_2 effectively, it will be necessary to know the thermodynamic properties of CO_2 + solute mixtures at supercritical conditions.

The isochoric heat capacity of mixtures near critical points is also interesting because the critical behavior of the mixture is governed by

an isomorphism principle. Therefore, precise isochoric heat-capacity measurements near the critical points of the mixture are extremely important to examine the consequences of the isomorphism principle on the critical behavior of $CO_2 + n$-decane mixtures. Binary mixtures of CO_2 with n-alkanes belong to three different types in the well known classification by van Konynenburg and Scott [11]. In this scheme, the systems CO_2 + (C_2 to C_4) are Type I (Horstmann et al. [12]), CO_2 + n-C_8 and CO_2 + n-C_{10} are Type II (Horstmann et al. [12] and Schneider [13,14]), and CO_2 + n-C_{16} (Horstmann et al. [12] and Schneider [15]) is Type III. This illustrates the possible complexity that can be observed experimentally for binary mixtures of this class.

Thermodynamic properties of $CO_2 + n$-decane mixtures have been reviewed in our previous paper (Polikhronidi et al. [16]). Therefore, some of the thermodynamic data which will be used in this work are only briefly reviewed here. A literature survey revealed (see Polikhronidi et al. [16]) that there are no isochoric-heat capacity data for the $CO_2 + n$-decane mixtures, except for the data reported in our previous paper for the composition of 0.2633 mole fraction of n-decane. Thus, the main objectives of this work are: (1) to provide new reliable experimental isochoric heat-capacity data for $CO_2 + n$-decane mixtures in near- and supercritical conditions (at temperatures up to 568 K) and high pressures (up to 40 MPa) for the various compositions; (2) to extract the phase boundary (T_S, ρ_S, x) and the critical (T_C, ρ_C, x) properties data for the $CO_2 + n$-decane mixtures from isochoric heat capacity measurements near the phase transition points; and (3) to stringently test the principle of isomorphism of critical phenomena for the mixtures with new accurate $C_V VTx$ measurements on CO_2+ n-decane. The present results considerably expand the available thermodynamic data base for $CO_2 + n$-decane mixtures that are needed to develop a reliable equation of state for the calculation of thermodynamic properties.

Due to a scarcity of experimental ($PVTx$ and $C_V VTx$) data, it is not yet possible to understand the effect of the solvent's (CO_2) near-critical properties on the thermodynamic behavior of a $CO_2 + n$-decane mixture and to develop an accurate scaling-type of equation of state. Thus, in this work we report $C_V VTx$ properties of mixtures of 0.095 and 0.178 mole fraction of n-decane measured with a high-temperature, high-pressure, nearly constant-volume adiabatic calorimeter in the temperature range between 295 and 568 K and the density range from 83 to 658 $kg \cdot m^{-3}$. Previously, we have reported experimental data for the isochoric heat capacity of the pure components CO_2 [17,18], n-decane [19], and CO_2+ n-decane [16] mixture ($x = 0.2633$ mole fraction of n-decane) in the near-critical and supercritical regions. We have used the same apparatus to measure C_V for the $CO_2 + n$-decane mixture. Prior to this work, some

thermodynamic properties of $CO_2 + n$-decane mixtures have been reported by other investigators [20–26]. However, most of the available $PVTx$ and VLE data cover only limited ranges of temperature, pressure, and concentration. The critical properties for this mixture were reported by several authors [16,20–22,24,27] in the full range of concentration. The Krichevskii parameter for $CO_2 + n$-decane mixtures determined with different methods was reported in Refs 16 and 28–30.

2. EXPERIMENTAL

2.1. Construction of the Calorimeter, Principle of Operation, and Assessment of Uncertainty

Details of the apparatus, procedures and uncertainties of the measured quantities have been provided in previous publications [31–37] and were used without modification. Only a brief review will be given here. Basically, a layer of a semiconductor (Cu_2O) is placed between two concentric spherical vessels, and the system behaves as a highly sensitive thermoelement that can serve as a sensor detecting deviations from adiabatic conditions. The thermoelectrical power of the Cu_2O is very high ($1150\,\mu V \cdot K^{-1}$). This makes it possible to detect extremely small temperature differences (10^{-6} K) between the concentric spherical vessels. The semiconductor layer simultaneously plays the role of a buffer that transmits pressure from the thin inner calorimetric shell to the thicker outer shell, which makes it possible to increase the strength of the calorimeter without increasing its heat capacity. Adiabatic conditions are reliably maintained in this calorimeter (see Mursalov et al. [38]). Heat capacities at constant volume are obtained by measuring the heat (ΔQ) input necessary to raise the temperature (ΔT) of a mixture (m) contained in a spherical calorimeter. The uncertainty is 1.0 to 1.5% in the liquid phase, 3 to 4% in the vapor phase, and 2 to 3% at near-critical and supercritical conditions. The one (vapor-C''_{V1} and liquid-C'_{V1}) – phase and two (vapor + liquid, C''_{V2} and C'_{V2}) – phase heat capacities at saturation, the saturated temperature (T_S), and saturated liquid (ρ'_S) and vapor (ρ''_S) densities can also be measured for near-critical mixtures as discussed below (see Section 2.2). The heat capacity is obtained from measurements of the following quantities: m, mass of the fluid; ΔQ, electrical energy released by the inner heater; ΔT, temperature change resulting from addition of an energy ΔQ; and C_0, empty calorimeter heat capacity [31–37]:

$$C_V = \frac{1}{m}\left(\frac{\Delta Q}{\Delta T} - C_0\right), \tag{1}$$

where the empty calorimeter heat capacity was calculated from the equation,

$$C_0 = 0.1244T - 1.037 \times 10^{-4}T^2 + 60.12 \tag{2}$$

where T is in K and C_0 is in $J \cdot K^{-1}$. The values of the empty calorimeter heat capacity were determined as a function of temperature by using (calibration procedure) the reference heat capacity data for He^4 [39] which is well known with an uncertainty of 0.2%. The density of the sample at a given temperature T and pressure P is calculated from the simple relation,

$$\rho = m/V_{PT}, \tag{3}$$

where m is the filling mass of the sample in the calorimeter, $V_{PT} = \Delta V_T + \Delta V_P$ is the temperature- and pressure-dependent volume of the calorimeter. The temperature dependence of the calorimeter volume at fixed pressure was calculated as

$$\Delta V_T = V_{T_0}[1 + 3\alpha_T(T - T_0)], \tag{4}$$

where $V_{T_0} = 105.405 \pm 0.01\,cm^3$ is the volume of calorimeter at a reference temperature $T_0 = 293.65\,K$ and at atmospheric pressure and α_T is the thermal expansion coefficient of the calorimeter material (stainless steel 10X18H9T) as a function of temperature,

$$\begin{aligned}\alpha_T = {} & 14.6 \times 10^{-6} + 1.59 \times 10^{-8}(T - 273.15) - 0.23 \times 10^{-10}(T - 273.15)^2 \\ & + 0.013 \times 10^{-12}(T - 273.15)^3,\end{aligned} \tag{5}$$

where T is in K. The uncertainty in the α_T calculation is about 2%. The value of V_{T_0} was previously calibrated from the known density of a standard fluid (pure water) with well-known (uncertainty is 0.0001% at 0.1 MPa in the liquid phase) PVT values (IAPWS standard, Wagner and Pruß [40]). The pressure dependence of the calorimeter volume ΔV_P was calculated from the Love formula (Keyes and Smith [41]) for the sphere. The maximum uncertainty in density measurements is about 0.06%.

The uncertainty of temperature measurements was 15 mK (ITS-90). The absolute uncertainty in C_V due to departures from full adiabatic control is $0.013\,kJ \cdot K^{-1}$. The combined standard uncertainty related to the indirect character of the C_V measurements did not exceed 0.16%. The heat capacity was measured as a function of temperature at nearly constant density. The correction related to the non-isochoric behavior during heating is about 0.5

to 1.0% in the temperature range from 300 to 650 K. The calorimeter was filled at room temperature, sealed off, and heated along a quasi-isochore. Each run for a heat-capacity measurement was normally started in the two-phase (L-V) region and completed in the one-phase (L or V depending on the filling factor) region at its highest temperature or pressure. When making measurements near the critical point, the sample is vigorously mixed by using a stirrer made of a thin perforated foil of stainless steel.

2.2. Method of Quasi-Static Thermograms

The technique used to determine T_S and ρ_S on the coexistence curve and of measuring the heat capacity C_V on this curve is the method of quasi-static thermograms as described in detail in our previous publications [35–38,42–44]. The method of quasi-static thermograms makes it possible to obtain reliable phase transition temperatures, including a critical temperature, with an uncertainty of 0.02 K. The method of quasi-static thermograms (temperature *vs.* time, *T-t* plot) has been used to determine the location of the phase transition (L-V) boundaries for the $CO_2 + n$-decane mixtures near the critical points. The construction of the calorimeter described above (see Section 2.1) enables control of the thermodynamic state of the measuring system with two independent sensors, namely, (1) a resistance thermometer-PRT and (2) a layer of cuprous oxide surrounding the calorimetric vessel and serving as an adiabatic shield (integral adiabatic screen). Synchronous recordings of the PRT readings and of the sensor for adiabatic control allow one to follow the thermodynamic state of the sample upon approaching the phase transition. On intersecting any phase transition curve (L-V, L-L, L-S, V-S, L-V-S, L-L-V, L-L-S), the heat capacity is known to change discontinuously, leading to a sharp change in the thermogram slope dT/dt. The high sensitivity of cuprous oxide makes it possible to immediately identify the temperature changes on a strip-chart recorder. Temperature changes are recorded on a thermogram tape of a pen-recorder as a spike produced by the Cu_2O sensor and as a change of the thermogram slope.

It is well known (Sengers and Levelt Sengers [45]) that the isochoric heat-capacity jump ΔC_V diverges at the critical point as $\Delta C_V \propto (T - T_C)^{-\alpha}$, where $\alpha = 0.110$ is the universal critical exponent. Therefore, the difference between thermogram slopes, $[(dt/dT)_{VT-\varepsilon} - (dt/dT)_{VT+\varepsilon}] \propto \Delta C_V$ (Rowlinson and Swinton [46]), is very large (the deviation in thermogram slopes within 25 to 30%). This makes it easy to locate any type of phase transition occurring in the system under study near the critical point (see, for example, Refs 42–44). Use of *P-T* isochoric break-point or of *P-ρ* isothermal break-point techniques are less sensitive for locating a phase

transition in the critical region (see, for example, Refs 47–53) because changes of the slope of P-T isochores and P-ρ isotherms are very small, since the densities of the phases before and after a phase transition in the critical region become almost identical [47,48]. For example, for pure fluids the slopes of the critical isochore (P-T) in the two and one-phase regions are identical at the critical point, while for the near-critical isochores the differences between slopes before and after a phase-transition point are too small to exactly determine the break point of the isochore (P-T). The uncertainties in the critical parameters and the phase-transition point determination by using the "break-point" technique reported in other studies [47–53] are within 1.5–2.0 K in temperature and 0.2 to 5 MPa in pressure. Therefore, the method using quasi-static thermograms is more suitable and a very sensitive technique to accurately determine of phase-boundary properties rather than isochoric (P-T) and isothermal (P-ρ) break-point techniques in the critical region.

To check the method and confirm the reliability of a determination of phase transitions and critical-point parameters by means of the quasi-static thermogram technique, phase-transition temperature measurements were made in pure distilled water in our previous studies with the same apparatus [34,36,37]. We have measured the phase transition temperature $T_S = 647.104 \pm 0.003$ K for the near-critical filling density of 321.96 $kg \cdot m^{-3}$ (the critical density adopted by IAPWS for pure water is 322.00 $kg \cdot m^{-3}$ [40]) which is in very close agreement with the critical temperatures $T_C =$ 647.096 K adopted by the IAPWS formulation [40] for pure water. An agreement of 8 mK between the measured value and the IAPWS standard [40] for the phase transition temperature is within our uncertainty and helps to confirm the reliability of the quasi-static thermogram technique.

3. RESULTS AND DISCUSSION

Measurements of the isochoric heat capacity for two $CO_2 + n$-decane mixtures ($x = 0.095$ and 0.178 mole fraction of n-decane) were performed on nineteen (liquid and vapor) filling densities between 87 and 659 $kg \cdot m^{-3}$ for 0.095 mole fraction of n-decane and nine (liquid and vapor) densities between 83 and 458 $kg \cdot m^{-3}$ for the 0.178 mole fraction of n-decane mixture. The experimental temperature range was 295 to 568 K. Measured values of the heat-capacity C_{VX} for the one- and two-phase regions are presented in Table I. For each density the values of C_{VX} and T_S at the saturation curve were measured with the quasi-static thermogram technique. The experimental one-phase liquid (C'_{V1}) and vapor (C''_{V1}), two-phase liquid (C'_{V2})and vapor (C''_{V2}) data, and the values of the temperature (T_S) and the density (ρ_S) at saturation are presented in

Table I. Experimental Values of the One- and Two-Phase Isochoric Heat Capacities of $CO_2 + n$-Decane Mixtures

T (K)	C_{VX} ($kJ \cdot kg^{-1} \cdot K^{-1}$)	T (K)	C_{VX} ($kJ \cdot kg^{-1} \cdot K^{-1}$)	T (K)	C_{VX} ($kJ \cdot kg^{-1} \cdot K^{-1}$)
x = 0.095 mole fraction of *n*-decane					
$\rho = 658.8\ kg \cdot m^{-3}$		**$\rho = 622.7\ kg \cdot m^{-3}$**		**$\rho = 574.1\ kg \cdot m^{-3}$**	
309.189	9.759	307.341	10.17	307.464	10.38
309.558	9.827	308.942	9.969	315.310	9.898
312.133	9.592	321.378	9.052	317.500	9.655
317.500	9.065	326.673	8.533	329.067	8.696
319.200	9.085	329.306	8.424	339.500	8.202
320.652	8.956	334.252	7.997	352.785	7.561
330.977	8.035	345.243	7.486	353.360	7.499
337.143	7.654	348.037	7.499	362.182	7.419
338.088	7.633	350.705	7.327	363.765	7.411
339.150	7.654	351.514	7.394	364.798	7.348
339.394	7.582	351.862	7.365	364.966	7.327
339.735	7.607	**352.093[a]**	**7.369[a]**	366.607	7.432
339.759[a]	**7.599[a]**	**352.093[b]**	**6.406[b]**	367.456	7.323
339.759[b]	**6.397[b]**	352.497	6.389	368.246	7.381
339.806	6.356	352.900	6.356	**368.528[a]**	**7.369[a]**
340.207	6.368	354.629	6.318	**368.528[b]**	**6.850[b]**
340.442	6.356	364.004	6.067	368.830	6.825
341.357	6.318	380.809	5.732	369.767	6.737
342.319	6.330	393.658	5.757	385.016	5.979
348.734	6.100	**$\rho = 509.4\ kg \cdot m^{-3}$**		397.776	5.853
362.182	5.870	305.241	10.68	403.373	5.891
371.228	5.694	317.986	9.446	411.472	5.836
$\rho = 534.8\ kg \cdot m^{-3}$		334.066	8.206	**$\rho = 498.0\ kg \cdot m^{-3}$**	
313.468	10.19	350.242	7.486	304.004	10.15
326.194	9.048	367.173	7.231	315.553	9.638
341.967	7.968	382.168	7.256	330.022	8.332
351.167	7.591	389.514	7.386	348.618	7.478
358.073	7.377	390.934	7.402	359.446	7.281
371.690	7.339	391.152	7.319	374.365	7.151
381.485	7.294	392.462	7.352	382.600	7.172
382.258	7.369	**393.006[a]**	**7.340[a]**	390.934	7.419
383.031	7.390	**393.006[b]**	**6.699[b]**	392.897	7.298
383.142	7.327	393.223	6.548	394.744	7.411
383.363[a]	**7.377[a]**	394.419	6.356	396.262	7.369
383.363[b]	**6.925[b]**	395.937	6.389	396.804	7.247
383.809	6.578	404.765	6.096	396.911	7.310
384.114	6.515	410.305	6.138	**397.344[a]**	**7.348[a]**
385.788	6.536	416.643	6.029	**397.344[b]**	**6.636[b]**
387.653	6.364	423.546	5.991	397.668	6.582
401.334	6.067	432.244	6.000	398.317	6.619
406.901	5.991	438.186	5.962	399.396	6.448
440.428	5.929	452.331	5.979	410.942	6.130

Table I. (*Continued*)

T (K)	C_{VX} (kJ·kg^{-1}·K^{-1})	T (K)	C_{VX} (kJ·kg^{-1}·K^{-1})	T (K)	C_{VX} (kJ·kg^{-1}·K^{-1})
442.030	5.933	**$\rho = 398.3$ kg·m^{-3}**		422.509	6.029
$\rho = 477.6$ kg·m^{-3}		308.665	9.420	437.676	6.021
325.714	8.449	318.229	8.688	442.053	6.021
340.324	7.428	334.066	7.662	442.878	6.021
354.629	7.130	350.010	7.160	**$\rho = 374.7$kg·m^{-3}**	
371.902	7.201	365.475	6.971	318.229	8.466
385.567	7.197	381.716	7.013	333.829	7.591
398.641	7.428	394.201	7.063	349.547	7.197
400.688	7.444	407.536	7.302	365.362	6.921
402.407	7.411	415.250	7.448	379.711	6.896
404.122	7.377	417.169	7.528	392.462	6.942
404.551[a]	**7.390**[a]	419.363	7.520	422.300	7.490
404.551[b]	**6.573**[b]	421.465	7.561	434.298	7.654
404.979	6.511	423.548	7.633	436.348	7.737
405.407	6.452	424.799	7.570	438.186	7.775
407.328	6.360	425.942	7.582	440.426	7.733
416.012	6.192	427.704	7.645	442.053	7.712
428.945	6.025	429.152	7.603	442.256	7.687
442.662	6.042	430.494	7.578	**442.459**[a]	**7.704**[a]
459.005	6.067	431.627	7.712	**442.459**[b]	**6.532**[b]
470.718	6.117	433.477	7.683	443.068	6.452
$\rho = 349.4$kg·m^{-3}		433.683	1.830	443.675	6.439
339.501	7.352	**433.991**[a]	**7.641**[a]	444.485	6.427
353.707	6.967	**433.991**[b]	**6.511**[b]	457.120	6.389
371.228	6.904	434.607	6.460	468.762	6.305
392.243	6.996	434.911	6.423	477.523	6.331
409.243	7.105	436.961	6.431	486.191	6.326
425.423	7.402	449.123	6.205	494.955	6.427
440.224	7.804	463.258	6.264	506.252	6.448
441.241	7.775	476.942	6.314	517.591	6.527
449.926	8.014	490.584	6.322	532.440	6.649
450.026	7.934	500.904	6.368	**$\rho = 281.4$kg·m^{-3}**	
450.428	7.959	515.371	6.511	330.732	7.700
450.729[a]	**7.846**[a]	**$\rho = 320.2$kg·m^{-3}**		351.167	7.030
450.729[b]	**6.619**[b]	337.143	7.428	375.261	6.921
451.531	6.494	351.167	7.009	394.636	6.879
452.532	6.469	365.816	6.862	417.694	7.164
469.743	6.343	384.796	6.858	433.477	7.457
494.196	6.423	399.181	6.938	455.726	7.909
513.518	6.540	413.904	7.122	461.876	8.198
530.983	6.686	428.532	7.344	463.851	8.252
$\rho = 241.0$kg·m^{-3}		435.119	7.494	465.818	8.374
334.066	7.729	452.131	7.963	467.585	8.491
358.302	7.155	453.931	8.030	469.452	8.432
384.135	6.946	454.928	8.014	470.622	8.445

Table I. (*Continued*)

T (K)	C_{VX} (kJ·kg^{-1}·K^{-1})	T (K)	C_{VX} (kJ·kg^{-1}·K^{-1})	T (K)	C_{VX} (kJ·kg^{-1}·K^{-1})
404.551	7.155	456.733	8.106	470.717	8.390
426.668	7.457	458.907	8.169	**471.107**[a]	**8.227**[a]
439.817	7.587	459.105	8.118	**471.107**[b]	**6.938**[b]
458.907	8.135	459.303	8.072	471.204	6.766
471.693	8.587	459.699	8.143	471.693	6.745
478.297	8.704	459.799	8.051	471.888	6.720
478.685	8.734	**460.096**[a]	**8.014**[a]	473.252	6.578
480.037	8.767	**460.096**[b]	**6.741**[b]	485.042	6.607
480.616	8.596	460.393	6.640	491.536	6.565
481.001[a]	**8.646**[a]	460.691	6.586	515.186	6.624
481.001[b]	**7.453**[b]	460.888	6.561	523.116	6.661
481.772	7.130	476.361	6.423	538.245	6.779
481.965	7.093	493.627	6.467	550.482	6.925
483.311	6.942	507.562	6.494	560.287	7.000
495.523	6.908	522.565	6.615	**$\rho = 176.7$ kg·m^{-3}**	
512.403	6.938	524.218	6.586	332.404	8.587
530.253	7.038	537.702	6.716	357.156	7.809
559.754	7.289	550.124	6.762	383.473	7.834
568.429	7.377	561.352	6.933	405.834	8.030
$\rho = 155.0$ kg·m^{-3}		**$\rho = 201.8$ kg·m^{-3}**		429.358	8.457
320.894	9.785	313.166	8.780	452.932	9.111
348.851	8.357	337.616	7.687	475.585	9.818
374.589	8.035	364.682	7.402	487.148	9.998
397.668	8.311	384.135	7.314	487.244	9.931
422.092	8.692	407.541	7.486	487.531	10.02
422.717	8.805	430.597	7.951	487.578	9.843
445.495	9.353	454.534	8.432	487.769	10.06
465.425	10.17	474.031	9.207	487.913	9.567
484.176	10.66	482.734	9.240	487.961	9.722
484.561	10.50	483.695	9.186	**488.104**[a]	**9.462**[a]
484.944	10.56	484.273	9.077	**488.104**[b]	**8.416**[b]
485.328	10.45	485.041	9.245	488.486	8.190
485.711	10.54	485.711	9.157	488.581	8.022
486.095	10.40	**485.999**[a]	**9.044**[a]	488.677	8.139
486.574	10.38	**485.999**[b]	**7.938**[b]	488.868	8.093
487.052[a]	**10.17**[a]	486.478	7.725	489.059	7.984
487.052[b]	**9.152**[b]	486.958	7.675	495.334	7.947
487.148	8.864	487.152	7.465	513.704	8.177
487.339	8.658	505.503	7.448	43.841	8.453
487.530	8.499	524.035	7.444	561.174	8.411
487.721	8.290	543.481	7.536	**$\rho = 110.8$ kg·m^{-3}**	
487.961	8.374	**$\rho = 131.5$ kg·m^{-3}**		325.713	12.267
488.191	8.382	295.524	12.39	355.319	10.87
499.867	8.692	328.273	10.70	375.930	10.10

Table I. (*Continued*)

T (K)	C_{VX} (kJ·kg^{-1}·K^{-1})	T (K)	C_{VX} (kJ·kg^{-1}·K^{-1})	T (K)	C_{VX} (kJ·kg^{-1}·K^{-1})
513.518	8.809	352.999	9.312	400.042	10.07
519.251	8.843	380.423	8.910	425.423	10.95
533.712	8.767	403.578	9.316	446.908	11.85
550.840	8.663	428.268	9.940	469.153	13.11
$\rho = 87.0$kg·m^{-3}		452.930	10.72	473.058	13.27
297.531	15.54	476.990	11.48	473.836	13.00
320.410	13.72	480.285	11.59	474.662	13.09
345.359	12.59	480.672	11.43	475.292	12.92
368.753	11.74	481.068	11.52	475.390	12.70
392.462	11.86	**481.831**[a]	**11.35**[a]	**475.488**[a]	**12.64**[a]
414.537	12.30	**481.831**[b]	**10.33**[b]	**475.488**[b]	**11.60**[b]
437.370	13.67	482.023	9.709	475.973	11.15
448.518	14.44	482.408	9.768	476.118	11.23
450.335	14.55	483.372	9.906	476.329	11.08
452.436	14.73	486.964	9.935	476.749	11.07
453.531	14.86	496.555	10.28	477.329	11.15
454.230	14.92	515.860	10.38	499.869	11.53
455.726	15.05	535.312	10.61	514.104	11.79
459.105	15.19	556.370	10.38	521.278	11.67
460.074	15.24	–	–	536.977	13.00
460.789	15.30	–	–	–	–
461.283	15.42	–	–	–	–
461.481	15.37	–	–	–	–
462.272	15.24	–	–	–	–
462.764	15.09	–	–	–	–
463.061[a]	**14.91**[a]	–	–	–	–
463.061[b]	**13.78**[b]	–	–	–	–
463.258	13.36	–	–	–	–
463.652	12.85	–	–	–	–
463.850	12.90	–	–	–	–
464.047	12.96	–	–	–	–
465.425	12.95	–	–	–	–
467.193	13.25	–	–	–	–
494.765	14.07	–	–	–	–
516.112	13.89	–	–	–	–
532.985	13.64	–	–	–	–
550.124	13.36	–	–	–	–
$\rho = 457.5$kg·m^{-3}		**$\rho = 375.0$kg·m^{-3}**		**$\rho = 310.8$kg·m^{-3}**	
320.894	8.754	349.547	7.808	346.870	7.796
350.705	7.900	377.712	7.779	348.036	7.741
375.706	7.817	417.484	8.185	358.412	7.729
408.605	8.156	418.534	8.218	359.560	7.754
417.450	8.474	439.613	8.646	372.014	7.657
419.163	8.520	452.230	9.001	373.134	7.687

Table I. (*Continued*)

T (K)	C_{VX} (kJ·kg^{-1}·K^{-1})	T (K)	C_{VX} (kJ·kg^{-1}·K^{-1})	T (K)	C_{VX} (kJ·kg^{-1}·K^{-1})
		x = 0.178 mole fraction of *n*-decane.			
428.945	8.687	464.047	9.353	383.152	7.737
431.009	8.679	472.474	9.717	384.255	7.720
444.281	9.127	473.058	9.814	400.257	7.938
446.908	9.236	476.455	9.876	401.334	7.925
447.311	9.294	476.649	9.973	425.130	8.273
447.317[a]	**9.240**[a]	477.036	9.910	447.664	8.826
447.317[b]	**7.900**[b]	**477.058**[a]	**9.918**[a]	448.470	8.842
447.951	7.774	**477.058**[b]	**8.101**[b]	469.056	9.382
448.271	7.842	477.523	8.018	469.838	9.449
448.552	7.804	477.814	8.059	486.765	10.090
452.332	7.565	478.201	7.984	489.631	10.190
453.232	7.528	478.491	8.009	490.394	10.274
463.455	7.465	485.616	7.833	494.575	10.416
474.614	7.427	486.765	7.884	495.428	10.370
ρ = 408.8 kg·m^{-3}		493.437	7.787	496.168	10.316
326.434	8.252	494.386	7.833	496.168	10.333
377.934	7.804	500.057	7.796	496.942	10.278
417.274	8.218	**ρ = 339.4 kg·m^{-3}**		**497.073**[a]	**10.195**[a]
438.391	8.717	301.273	10.048	**497.073**[b]	**8.432**[b]
440.835	8.738	302.267	9.776	497.415	8.390
447.909	9.027	304.004	9.805	497.509	8.340
450.930	9.001	304.499	9.705	497.604	8.361
453.731	9.056	316.401	8.763	500.904	8.214
458.709	9.378	317.257	8.683	501.751	8.248
460.888	9.504	339.500	7.879	517.683	8.076
462.070	9.642	354.168	7.771	518.514	8.126
462.930	9.738	355.089	7.812	543.481	8.277
463.470	9.759	380.598	7.833	544.112	8.365
464.530	9.838	394.201	7.913	**ρ = 284.3 kg·m^{-3}**	
464.770	9.847	407.901	8.051	351.746	7.842
465.050	9.818	407.967	8.064	353.015	7.821
465.130[a]	**9.839**[a]	429.977	8.386	398.641	7.913
465.130[b]	**8.101**[b]	431.009	8.407	399.827	7.963
466.300	8.026	445.400	8.813	447.109	8.838
467.050	7.976	447.410	8.846	448.116	8.767
467.970	7.930	464.344	9.466	493.437	10.241
468.762	7.909	465.228	9.428	494.386	10.370
476.555	7.678	477.718	9.730	500.057	10.580
479.844	7.666	483.600	10.010	500.998	10.509
490.013	7.578	484.561	10.031	503.816	10.643
495.524	7.624	486.861	10.098	504.754	10.592
502.878	7.695	487.050	10.061	504.792	10.500
ρ = 164.2 kg·m^{-3}		487.721	10.082	**504.829**[a]	**10.425**[a]
350.242	10.015	488.277	10.069	**504.829**[b]	**8.729**[b]

Table I. (*Continued*)

T (K)	C_{VX} ($kJ \cdot kg^{-1} \cdot K^{-1}$)	T (K)	C_{VX} ($kJ \cdot kg^{-1} \cdot K^{-1}$)	T (K)	C_{VX} ($kJ \cdot kg^{-1} \cdot K^{-1}$)
376.460	9.805	**488.424**[a]	**10.031**[a]	504.885	8.679
408.179	10.136	**488.424**[b]	**8.227**[b]	505.960	8.524
456.523	11.350	488.820	8.135	506.316	8.482
457.517	11.325	489.440	8.110	508.720	8.348
494.386	12.430	493.437	8.013	509.654	8.348
507.001	12.815	494.291	8.030	544.381	8.411
512.218	13.159	503.066	7.959	**$\rho = 83.3\ kg \cdot m^{-3}$**	
515.741	13.104	503.817	8.005	337.379	19.564
519.067	13.376	512.218	7.946	457.166	19.284
521.093	13.284	512.961	7.959	497.595	20.192
521.277	13.155	530.668	8.013	502.502	20.481
521.646	12.928	531.397	8.030	504.285	20.234
522.198[a]	**12.707**[a]	**$\rho = 117.8\ kg \cdot m^{-3}$**		505.784	20.414
522.198[b]	**11.199**[b]	305.736	13.615	508.120	20.029
523.668	10.986	306.725	13.490	509.240	19.581
524.035	10.856	357.156	12.305	510.264	19.807
524.403	10.731	358.531	12.074	512.217	19.636
529.614	10.366	406.261	12.334	513.332	19.384
530.071	10.345	448.117	13.422	513.704	18.878
530.618	10.274	480.808	14.758	514.445	18.530
535.891	10.262	481.772	14.901	**515.001**[a]	**18.266**[a]
554.056	10.136	500.810	15.495	**515.001**[b]	**16.102**[b]
–	–	501.563	15.583	516.757	15.868
–	–	501.690	15.671	517.480	16.002
–	–	503.629	15.721	524.768	15.981
–	–	516.201	15.336	535.395	15.579
–	–	517.036	15.646	536.163	15.809
–	–	517.775	15.415	536.977	15.834
–	–	518.790	15.093	546.627	15.801
–	–	519.251	14.645	547.615	16.144
–	–	**519.436**[a]	**14.595**[a]	556.908	16.223
–	–	**519.436**[b]	**12.920**[b]	–	–
–	–	520.725	12.824	–	–
–	–	526.601	12.669	–	–
–	–	528.428	12.610	–	–
–	–	529.706	12.501	–	–
–	–	533.167	12.334	–	–
–	–	534.076	12.275	–	–
–	–	546.368	12.338	–	–

[a] Two-phase saturation experimental points.
[b] One-phase saturation experimental points.

Table II. Some experimental results for C_{VX} at selected isochores in the one- and two-phase regions for liquid and vapor densities as a function of temperature are shown in Figs 1 to 4. As shown in Figs 1 to 3, for each isochore, the two-phase heat capacity C_{VX} drops discontinuously at the phase-transition temperature T_S to a value corresponding to that of the one-phase region. For each density at the phase-transition point T_S, we have two values of the heat capacity, namely C_{VS1} and C_{VS2}, corresponding to one- and two-phase states, respectively. By changing the amount of sample in the calorimeter, it is possible to obtain a complete set of T_S, C_{VS1}, and C_{VS2} data at saturation (saturation curve). Thus, the C_{VX} experiments provide useful information about the saturation properties (T_S, ρ_S, C_{VS1}, and C_{VS2}) near the critical point and, as a result, the values of the critical properties (T_C, ρ_C) of the mixture. Figure 3 depicts the temperature dependence of the measured values of the isochoric heat capacities for the $CO_2 + n$-decane mixtures at constant compositions and constant near-critical and critical densities. Figure 3 (left) shows the temperature dependence of C_{VX} at constant concentrations and almost the same fixed densities. This figure demonstrates how the phase transition temperature changes with composition along the same isochore. Figure 4 shows one-phase isochoric heat capacities along selected liquid and vapor isochores near the coexistence curves.

Several events occur when the fluid or fluid mixture is heated isochorically. Heating the pure fluids or fluid mixtures (completely miscible mixtures) in equilibrium with a vapor can lead to two different sequences of phase transitions, depending on the fill coefficient or the average fill density. The fill coefficient is defined as the ratio of the volume of the mixture to the volume of the vessel at ambient temperature. The average density equals the ratio of the mass of the mixture to the volume of the vessel at ambient temperature. A sequence of experimental data for the heat capacity of the two-phase system obtained at a given average density will be called an isochore, even though the volume occupied by the mixture is not strictly constant during an experimental run, due to the thermal expansion of the calorimeter vessel. At the highest measured densities ($\rho > \rho_C$), the liquid phase expands on heating and fills the entire vessel, while the vapor phase disappears. A transition (L-G$\Leftrightarrow$L) occurs, with a drop in heat capacity as the number of phases decreases (see Figs 1 to 3). At low measured densities ($\rho < \rho_C$), the vapor phase expands on heating and fills the entire vessel, while the liquid phase disappears. A transition takes place from two- to one-phase equilibrium (L-G$\Leftrightarrow$G), again with a drop of the heat capacity (see Figs 1 to 3). In more complicated systems (for example, water + salt solutions with salt precipitation at high temperatures [43,44] or partially miscible liquids like water + hydrocarbon mixtures [42]) other

Table II. Experimental Values of the One- and Two-Phase Liquid (C'_{V1}, C'_{V2}) and Vapor (C''_{V1}, C''_{V2}) Isochoric Heat Capacities, Temperatures (T_S), and Densities (ρ'_S, ρ''_S) of $CO_2 + n$-Decane Mixtures Along the Saturation Curve

T_S (K)	ρ'_S ($kg \cdot m^{-3}$)	C'_{V1} ($kJ \cdot kg^{-1} \cdot K^{-1}$)	C'_{V2} ($kJ \cdot kg^{-1} \cdot K^{-1}$)
	$x = 0.095$ mole fraction of n-decane		
339.759	658.8	6.397	7.599
352.093	622.7	6.406	7.369
368.528	574.1	6.850	7.369
T_S (K)	ρ''_S ($kg \cdot m^{-3}$)	C''_{V1} ($kJ \cdot kg^{-1} \cdot K^{-1}$)	C''_{V2} ($kJ \cdot kg^{-1} \cdot K^{-1}$)
383.363	534.8	6.925	7.377
393.006	509.4	6.699	7.340
397.344	498.0	6.636	7.348
404.551	477.6	6.573	7.390
433.991	398.3	6.511	7.641
442.459	374.7	6.532	7.704
450.729	349.4	6.619	7.846
460.096	320.2	6.741	8.014
471.107	281.4	6.938	8.227
481.001	241.0	7.453	8.646
485.999	201.8	7.938	9.044
488.104	176.7	8.416	9.462
487.052	155.0	9.152	10.17
481.831	131.5	10.33	11.35
475.488	110.8	11.60	12.64
463.061	87.03	13.78	14.91
T_S (K)	ρ'_S ($kg \cdot m^{-3}$)	C'_{V2} ($kJ \cdot kg^{-1} \cdot K^{-1}$)	C'_{V1} ($kJ \cdot kg^{-1} \cdot K^{-1}$)
	$x = 0.178$ mole fraction of n-decane		
447.317	457.50	9.240	7.900
451.390	445.04	9.336	7.938
457.767	426.08	9.688	8.118
460.150	420.00	9.855	8.218
T_S (K)	ρ''_S ($kg \cdot m^{-3}$)	C''_{V2} ($kJ \cdot kg^{-1} \cdot K^{-1}$)	C''_{V1} ($kJ \cdot kg^{-1} \cdot K^{-1}$)
464.130	408.8	9.860	8.122
477.058	375.0	9.918	8.101
488.424	339.4	10.031	8.227
497.073	310.8	10.195	8.432
504.829	284.3	10.425	8.729
522.198	164.2	12.707	11.199
519.436	117.8	14.595	12.920
515.001	83.31	18.266	16.102

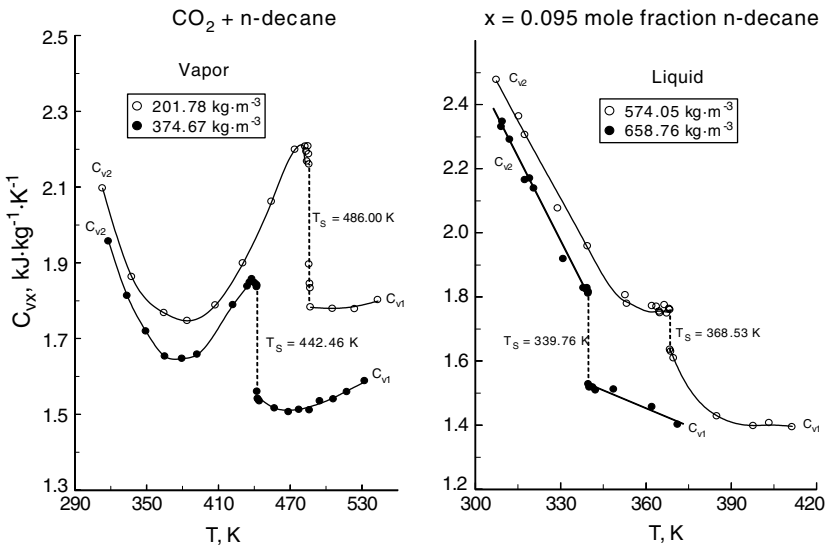

Fig. 1. Experimental one- and two-phase isochoric heat capacities of $CO_2 + n$-decane as a function of temperature on liquid and vapor and near-critical isochores for $x = 0.095$ mole fraction of n-decane. Dashed lines are isochoric heat capacity jumps at the phase transition temperatures for each density. Solid lines are guides for the eye.

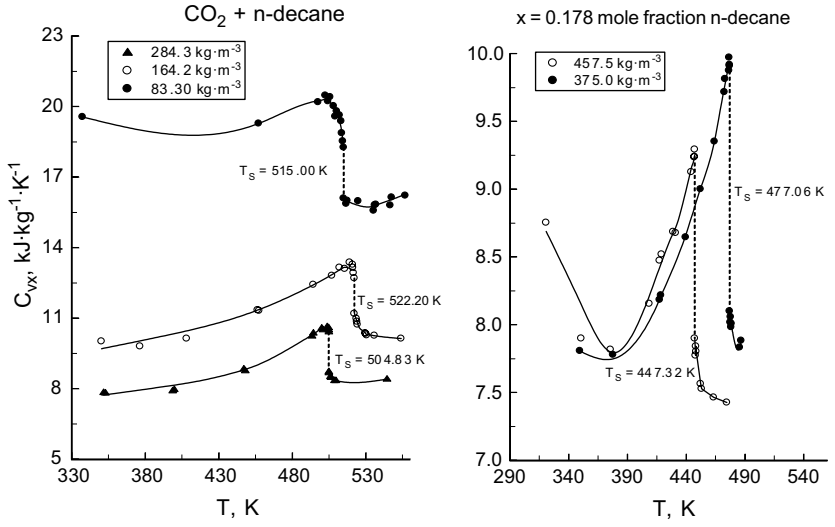

Fig. 2. Experimental one- and two-phase isochoric heat capacities of $CO_2 + n$-decane as a function of temperature on near-critical vapor isochores for $x = 0.178$ mole fraction of n-decane. Dashed lines are isochoric heat capacity jumps at the phase transition temperatures for each density. Solid lines are guides for the eye.

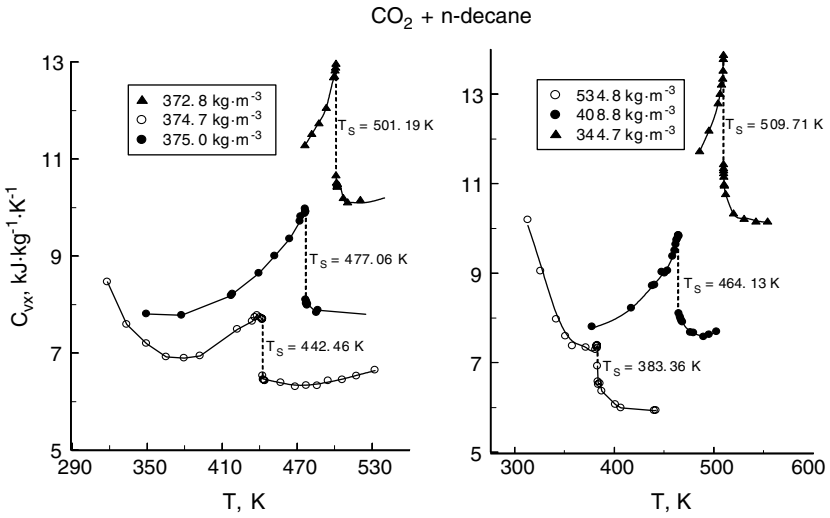

Fig. 3. Experimental one- and two-phase isochoric heat capacities of $CO_2 + n$-decane as a function of temperature for selected constant densities and the critical isochores for the various compositions; •, $x = 0.178$ (this work); ○, $x = 0.095$ (this work); ▲, $x = 0.263$ (Polikhronidi et al. [16]). Solid lines are guides for the eye.

sequences of phase transitions like L-V-S, L-L-S, L-L-V are possible (see, for example, Abdulagatov et al. [44], Valyshko et al. [43], and Kamilov et al. [42]).

The dependence of the two-phase isochoric heat capacities of the $CO_2 + n$-decane mixtures on the specific volume along three selected isotherms and constant composition is shown in Fig. 5. As this figure shows, the two-phase $C_{VX} - V$ isotherms (right of phase transition in Fig. 5) exhibit a minimum at a volume near $3.0\,\mathrm{cm^3 \cdot g^{-1}}$ and a maximum is exhibited at a volume of about $1.87\,\mathrm{cm^3 \cdot g^{-1}}$ which is very close to the value of the critical specific volume $V_C = 1.82\,\mathrm{cm^3 \cdot g^{-1}}$ for this composition (0.095 mole fraction of *n*-decane). Figures 6 and 7 illustrate the temperature dependence of the liquid and vapor one- and two-phase isochoric heat capacities of the $CO_2 + n$-decane mixture at saturation. As shown in Fig. 7, which depicts the temperature ($C'_{V1} - T$ and $C''_{V1} - T$) dependence of the one-phase liquid and vapor isochoric heat capacities at saturation, a cusp (liquid-vapor critical point) was observed for the mixture. It is shown that while C'_{V1} and C''_{V1} increases monotonically with T up to the critical point, an abrupt change of the slope is observed at the cusp (critical point). At this cusp, the liquid and vapor become identical, providing the temperature, density, and concentrations of the critical points of the mixture.

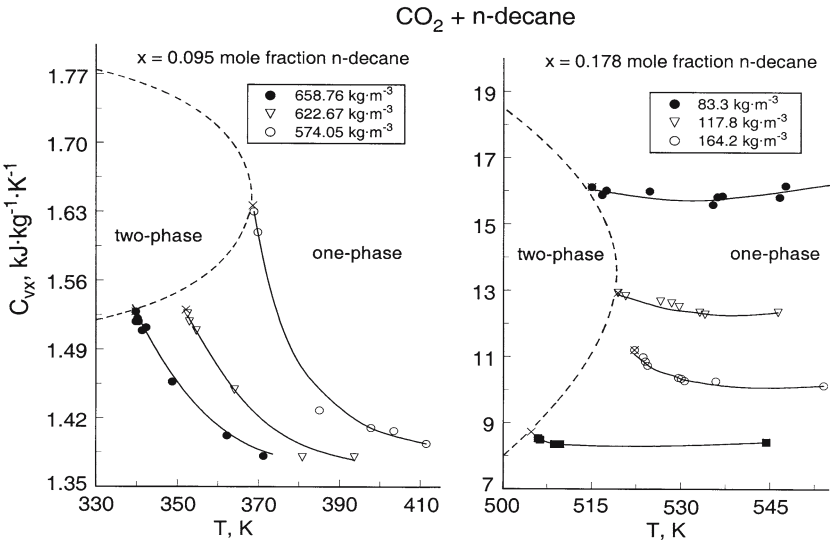

Fig. 4. Experimental one-phase isochoric heat capacities of $CO_2 + n$-decane as a function of temperature along the selected liquid and vapor densities near the phase transition curves for various compositions. Solid lines are guides for the eye.

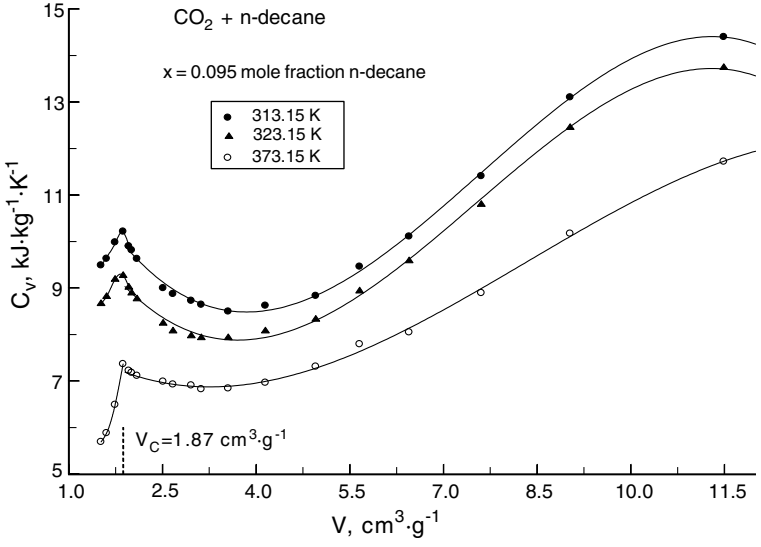

Fig. 5. Experimental two-phase isochoric heat capacities of $CO_2 + n$-decane as a function of specific volume on three selected near-critical isotherms. Solid lines are guides for the eye.

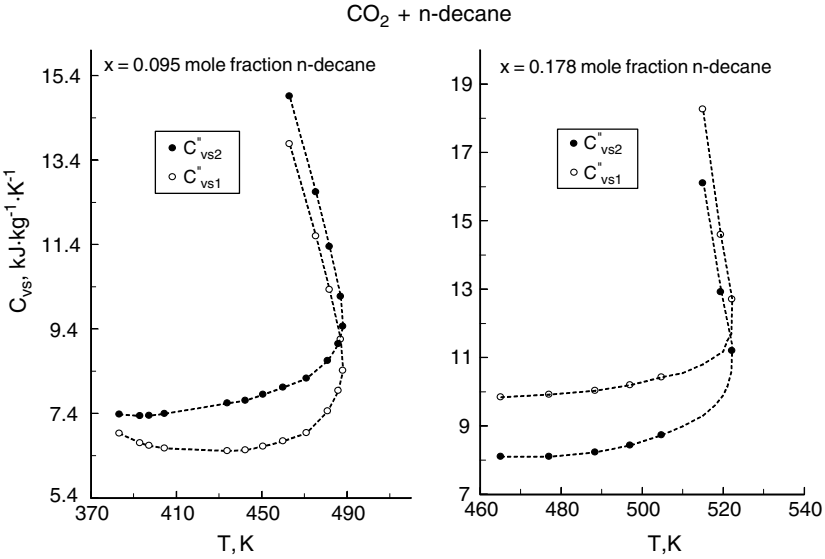

Fig. 6. Experimental values of vapor one-phase (C''_{V1}) and two-phase (C''_{V2}) isochoric heat capacities on the coexistence curve as a function of temperature. Dashed lines are guides for the eye.

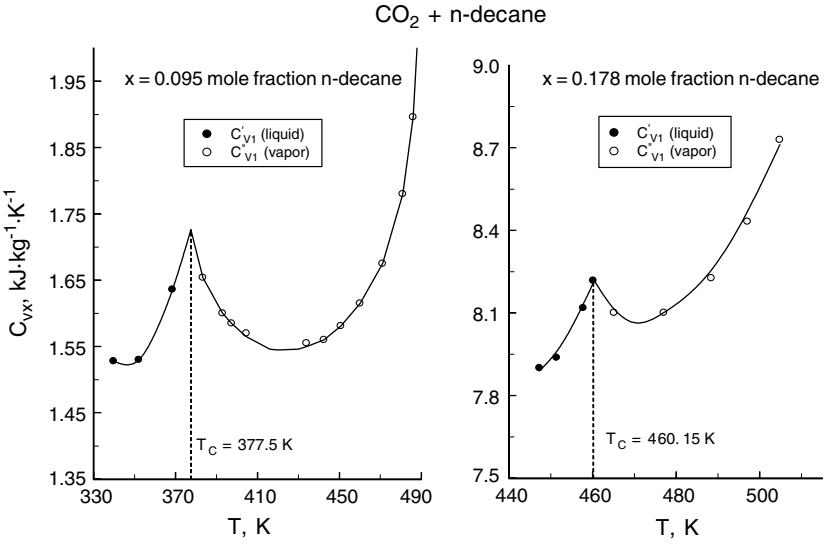

Fig. 7. Experimental values of liquid and vapor one-phase(C'_{V1}, C''_{V1}) isochoric heat capacities on the coexistence curve as a function of temperature for various compositions near the critical points (break - points). Solid lines are guides for the eye.

Figure 8 demonstrates the liquid ($\Delta C'_{VX}$) and vapor ($\Delta C''_{VX}$) isochoric heat capacity jumps as a function of temperature near the critical point for a composition of 0.095 mole fraction of *n*-decane. From our experimental C_{VX} and $(T_S - \rho_S)$ measurements on the coexistence curve for $CO_2 + n$-decane mixtures, we have deduced the values for the critical temperature T_C and the critical density ρ_C. Our results are presented in Table III. The critical-property data obtained are in fair agreement with data reported by Reamer and Sage [20] at nearly the same compositions.

A more detailed comparison of various critical property data sets for $CO_2 + n$-decane mixtures has been given in our previous paper

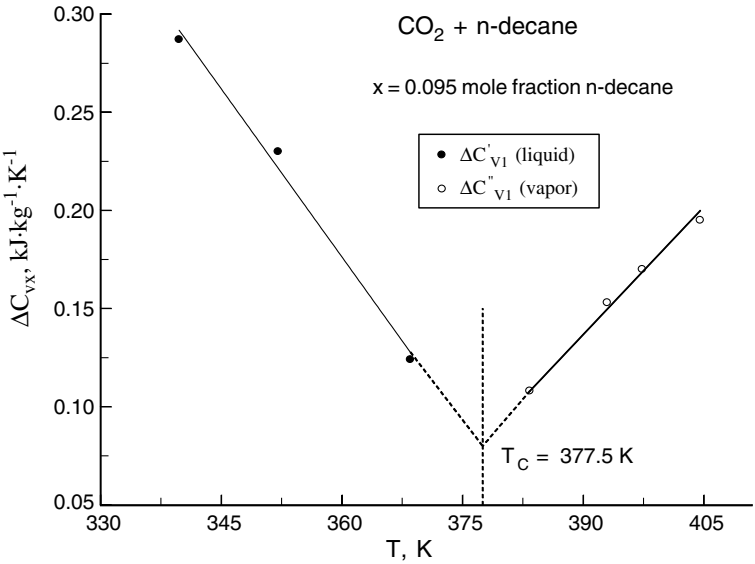

Fig. 8. Experimental values of liquid ($\Delta C'_{VX}$) and vapor ($\Delta C''_{VX}$) isochoric heat capacity jumps as a function of temperature near the critical point at fixed composition.

Table III. Critical Properties of $CO_2 + n$-Decane Mixtures from Calorimetric Measurements

x (mole fr.)	T_C (K)	ρ_C ($kg \cdot m^{-3}$)	P_C (MPa)
0.095	377.50	551.0	16.25
0.178	460.15	420.0	18.23
0.263[a]	509.71[a]	344.7[a]	15.37[a]

[a] Polikhronidi et al. [16]

(Polikhronidi et al. [16]). Table IV lists the present critical data together with the data reported by other investigators. As one can see, the consistency between this work and the published data for the critical parameters is good, except for the data reported by Reamer and Sage [20] for the critical densities at low concentrations of *n*-decane. For a composition of 0.095 mole fraction of *n*-decane, the difference between the present critical temperature and the data reported by Reamer and Sage [20] is 0.12 K, an amount that is very close to their uncertainty (see Table IV). Good agreement, within 0.52%, was found between the critical density reported by Nagarajan and Robinson [21], while the difference between the present value of the critical density and that reported by Reamer and Sage [20] is about 8.5% at 0.095 mole fraction of *n*-decane. Good agreement of 0.06% was found between the critical pressure reported by Reamer and Sage [20] and Nagarajan and Robinson [21] and the present result. For the composition of 0.178 mole fraction *n*-decane, the differences between the present critical temperature and critical density and the values reported by Reamer and Sage [20] are 0.79 K and 0.30 $kg \cdot m^{-3}$, respectively. The difference between the critical pressures for this composition is 0.77%, while the value of the critical pressure by Nagarajan and Robinson [21] differs from the present value by 0.6%. The critical density reported by Gulari et al. [22] for $CO_2 + n$-decane mixtures differs from the present result by about 2% (the present result is systematically lower).

In this work, closely spaced measurements were made in the critical region and near every phase transition point, providing essential information for an accurate determination of both the critical parameters and of the saturation temperatures and densities near the critical point. Figure 9 shows the measured vapor-liquid coexistence curve ($T_S - \rho_S$) data for the $CO_2 + n$-decane mixtures along with the vapor-liquid coexistence

Table IV. Comparison Between Experimental Critical Properties and Values Reported by other Authors for $CO_2 + n$-Decane Mixtures

T_c (K)	ρ_c ($kg \cdot m^{-3}$) This work	P_c (MPa) This work	T_c (K) Reamer and Sage [20]	ρ_c ($kg \cdot m^{-3}$) Reamer and Sage [20]	P_c (MPa) Reamer and Sage [20]	P_c (MPa) Nagarajan and Robinson [21]	ρ_c ($kg \cdot m^{-3}$) Nagarajan and Robinson [21]
			x = 0.095 mole fraction of *n*-decane				
377.5	551.0	16.50	377.62	507.4	16.49	16.49	553.5
			x = 0.178 mole fraction of *n*-decane				
460.15	420.0	18.23	459.36	419.7	18.09	18.34	–

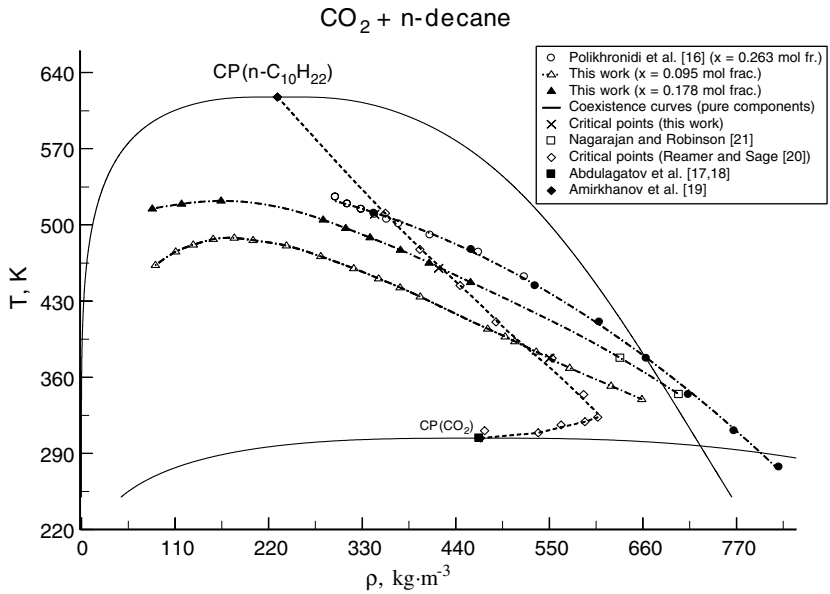

Fig. 9. Experimental liquid and vapor densities at saturation for $CO_2 + n$-decane mixtures and their pure components from C_{VX} experiments (quasi-static thermogram technique). Dashed lines are guides for the eye.

curves of both pure components near the critical point calculated with the Lemmon and Span [54] (*n*-decane) and Span and Wagner [55] (CO_2) multiparameter equations of state. Figure 9 also includes the data reported by Reamer and Sage [20] and Nagarajan and Robinson [21] on the coexistence curves. This figure demonstrates that the consistency between the present and published $T_S - \rho_S$ data is satisfactory. As one can see from Fig. 9, the shape of the liquid-vapor coexistence curve near the critical point for a mixture differs dramatically from the flat top of the dome seen for pure fluids. Figure 9 also shows the loci of critical points (in $T_C - \rho_C$ projection) reported by other authors together with our results. As one can see from this figure, the $T_C - \rho_C$ projection of the critical curve exhibits a density maximum near $600\,\mathrm{kg \cdot m^{-3}}$. The same behavior of the $T_C - \rho_C$ projection of the critical curve has been found for other CO_2+ hydrocarbon mixtures [56]. A very small, but noticeable, anomaly of the liquid-vapor coexistence curve can be seen near the critical point in the $T_S - \rho_S$ plane (see Fig. 9) that would be difficult to detect by means of $PVTx$ experiments alone. The shape of the liquid-vapor coexistence curve near the critical point has two inflection points which bracket the

critical point (Rainwater [57]). The critical point for this mixture does not coincide with the maximum temperature point, $\left(\frac{\partial T_S}{\partial \rho_S}\right)_x \neq 0$, of the liquid-vapor coexistence curve. This is why few investigators report this anomalous behavior which has been discussed from a theoretical perspective by Rainwater [57].

In our previous publication (Polikhronidi et al. [16]), we discussed in detail the results of the interpretation of the critical anomaly of the isochoric heat capacity for the $CO_2 + n$-decane mixture ($x = 0.2633$ mole fraction of n-decane) in terms of renormalization theory (Anisimov et al. [58–61]). According to the isomorphism principle, the near-critical behavior of binary fluids is controlled by two characteristic system-dependent parameters, K_1 and K_2, which are determined by the initial slope ($x \to 0$) of the critical curves ($T_C - x$) and ($P_C - x$) (see Anisimov et al. [58–61]). The parameter K_1 controls strongly divergent properties such as the isothermal compressibility K_T and the isobaric heat capacity C_P, while the parameter K_2 controls the weakly divergent properties like the isochoric heat capacity C_V and defines the range of Fisher renormalization of the critical exponents [62]. The parameters K_1 and K_2 are defined [63] by

$$K_1 = \frac{x(1-x)}{\rho_C R T_C}\left[\frac{dP_C}{dx} - \left(\frac{dP_S}{dT}\right)^c_{CxC}\frac{dT_C}{dx}\right] \quad \text{and}$$

$$K_2 = \frac{x(1-x)}{T_C}\frac{dT_C}{dx}. \tag{6}$$

Correspondingly, two characteristic temperature differences, τ_1 and τ_2, and two characteristic density differences, $\Delta\bar{\rho}_1$ and $\Delta\bar{\rho}_2$, are defined through K_1 and K_2:

$$\tau_1 = \left[\frac{\Gamma_0^+ K_1^2}{x(1-x)}\right]^{1/\gamma}, \quad \tau_2 = \left[\frac{A_0^+ K_2^2}{x(1-x)}\right]^{1/\alpha}, \tag{7}$$

$$\Delta\bar{\rho}_1 = B_0 \tau_1^\beta, \quad \Delta\bar{\rho}_2 = B_0 \tau_2^\beta, \tag{8}$$

where $\tau = (T_C - T)/T_C$ and $\Delta\rho = (\rho_C - \rho)/\rho_C$. For CO_2, the asymptotic critical amplitudes of the power laws for isochoric heat capacity, the coexistence curve, and the isothermal compressibility are, respectively, $A_0^+ = 26.36$, $B_0 = 1.708$, and $\Gamma_0^+ = 0.056$ [64], and the universal critical exponents for C_V are $\alpha = 0.110$ and for the coexistence curve $\beta = 0.325$ [45]. In the dilute-solution limit ($x \to 0$), the expression between the brackets in Eq. (6) for K_1 reduces to the Krichevskii parameter [63,65–67],

$$K_{\mathrm{kr}} = \lim_{X\to 0}\left(\frac{\partial P}{\partial x}\right)^{C}_{V_C T_C} = \left(\frac{\partial P}{\partial x}\right)^{C}_{V_C T_C} = \left(\frac{\partial P_c}{\partial x}\right)^{C}_{CRL} - \left(\frac{dP_S}{dT}\right)^{C}_{CXC}\left(\frac{\partial T_c}{\partial x}\right)^{C}_{CRL}. \tag{9}$$

To calculate the values of $\frac{\mathrm{d}T_C}{\mathrm{d}x}$ and $\frac{\mathrm{d}P_C}{\mathrm{d}x}$, the present and published (Reamer and Sage [20], Nagarajan and Robinson [21], and Gulari et al. [22]) experimental critical curve data for the $CO_2 + n$-decane mixture were fitted to a polynomial function for the critical temperatures and critical pressures as a function of composition:

$$T_C(x) = T_C(CO_2) + \left(\frac{\mathrm{d}T_C}{\mathrm{d}x}\right)_{x=0} x + T_1 x^2 + \cdots, \tag{10}$$

$$P_C(x) = P_C(CO_2) + \left(\frac{\mathrm{d}P_C}{\mathrm{d}x}\right)_{x=0} x + P_1 x^2 + \cdots, \tag{11}$$

where $T_C(CO_2) = 304.136\,\mathrm{K}$ and $P_C(CO_2) = 7.3773\,\mathrm{MPa}$ are the critical temperature and the critical pressure of pure carbon dioxide (Span and Wagner [55]); $\left(\frac{\mathrm{d}T_C}{\mathrm{d}x}\right)_{x=0} = 1173.8\,\mathrm{K}$ and $\left(\frac{\mathrm{d}P_C}{\mathrm{d}x}\right)_{x=0} = 126.2\,\mathrm{MPa}$. The quantity $\left(\frac{\mathrm{d}P_S}{\mathrm{d}T}\right)^{C}_{C\times C} = 0.1712\,\mathrm{MPa}\cdot\mathrm{K}^{-1}$, which is the slope of the vapor pressure curve of the solvent (carbon dioxide) at the critical point, was calculated with the aid of the vapor-pressure correlation of Span and Wagner [55]. The values of the initial critical locus slopes for the $CO_2 + n$-decane mixture at infinite dilution ($x \to 0$) were determined by using the fitting procedure from Eqs (10) and (11). The values of the derivatives $\frac{\mathrm{d}T_C}{\mathrm{d}x} = 724 \pm 15\,\mathrm{K}$, $\frac{\mathrm{d}P_C}{\mathrm{d}x} = 96 \pm 3\,\mathrm{MPa}$ for the composition of $x = 0.095$ mole fraction of n-decane and $\frac{\mathrm{d}T_C}{\mathrm{d}x} = 1200 \pm 25\,\mathrm{K}$, $\frac{\mathrm{d}P_C}{\mathrm{d}x} = 10 \pm 1\,\mathrm{MPa}$ for the composition of 0.178 mole fraction of n-decane were also derived from Eqs (10) and (11). These values of $\frac{\mathrm{d}T_C}{\mathrm{d}x}$ and $\frac{\mathrm{d}P_C}{\mathrm{d}x}$ together with critical amplitudes ($A_0^+ = 26.36$, $B_0 = 1.708$, and $\Gamma_0^+ = 0.056$) were used to calculate the characteristic parameters (K_1, K_2, τ_1, τ_2, $\Delta\bar{\rho}_1$, and $\Delta\bar{\rho}_2$) from Eqs (6) to (8). As one can see from Eq. (6), the parameter K_1 vanishes at the critical azeotrope, while K_2 vanishes at the critical temperature extreme, $\frac{\mathrm{d}T_C}{\mathrm{d}x} = 0$, so that the characteristic temperatures (τ_1 and τ_2) are equal to zero at these points. The calculated values of derivatives $\left(\frac{\mathrm{d}T_C}{\mathrm{d}x}\right)_{x=0} = 1173.8\,\mathrm{K}$ and $\left(\frac{\mathrm{d}P_C}{\mathrm{d}x}\right)_{x=0} = 126.2\,\mathrm{MPa}$ at infinite dilution ($x \to 0$) with Eqs (10) and (11) were used to determine the value of the Krichevskii parameter for the $CO_2 + n$-decane mixture. Our result

for the Krichevskii parameter (−74.75 MPa) agrees (deviations within ±1.0%) with the value reported by other authors [16,28–30] from the critical properties, solubility, and supercritical-fluid chromatography data. This good agreement between present and published values of the Krichevskii parameter confirms the reliability and accuracy of the calculated values of the derivatives, $\frac{dT_C}{dx}$ and $\frac{dP_C}{dx}$, from Eqs (10) and (11) and correct calculations of the characteristic parameters (K_1, K_2, τ_1, τ_2, $\Delta\bar{\rho}_1$, and $\Delta\bar{\rho}_2$) from Eqs (6) to (8) using these values.

According to the isomorphism principle [58–61], along the critical isochore in the one-phase region, all properties of a binary fluid mixture will exhibit the same behavior as those of a pure fluid in a range of temperatures, $\tau \gg \tau_1$ and $\tau \gg \tau_2$. At $\tau_2 < \tau < \tau_1$, properties that exhibit strong singularities in one-component fluids (associated with the critical exponent γ) will reach a plateau, while, weakly singular properties (associated with the critical exponent α) will continue to grow. At $\tau < \tau_2$, those properties that diverge weakly in one-component fluids will be saturated, and all critical exponents will be renormalized by the factor $1/(1-\alpha)$. In terms of density along the critical isotherm, the behavior of all properties will be one-component-like at densities $|\Delta\bar{\rho}| \gg \pm\Delta\bar{\rho}_1$ ("-" for the $\rho > \rho_C$ and "+" for the $\rho < \rho_C$) and the Fisher renormalization occurs at $|\Delta\bar{\rho}| \ll \pm\Delta\bar{\rho}_2$ [62]. At $\tau \ll \tau_2$, the behavior of the isochoric heat capacity of a binary mixture will be renormalized by a factor $1/(1-\alpha)$ (Fisher renormalization [62]). In terms of density along the critical isotherm the behavior of the isochoric heat capacity will be renormalized at densities $|\Delta\rho| \ll \Delta\rho_2$.

The values of the characteristic parameters K_1, τ_1, K_2, τ_2, $\Delta\rho_1$, and $\Delta\rho_2$ calculated from Eqs (6) to (11) for a $CO_2 + n$-decane mixture for the present compositions is given in Table V. As one can see from Table V, the values of the characteristic temperature τ_2 for both compositions ($x = 0.095$ and $x = 0.178$ mole fraction of n-decane) are too large. The slope of the critical temperature T_C as a function of x at concentrations of 0.095 and 0.178 mole fractions of n-decane is steep enough that a renormalization of the critical exponents can be observed for this mixture at temperatures below τ_2 and at the critical density. Figure 10 shows the concentration dependence of the characteristic temperature (τ_1) and the characteristic density differences ($\Delta\bar{\rho}_1$, $\Delta\bar{\rho}_2$) for the $CO_2 + n$-decane mixtures. The characteristic temperatures and densities (τ_2, $\Delta\bar{\rho}_2$) change rapidly with increasing concentration of n-decane, while the values of (τ_1 and $\Delta\bar{\rho}_1$) change very weakly (see Table V and Fig. 10). Therefore, the temperatures τ measured in this work are significantly lower than τ_2 ($\tau \ll \tau_2$, experimentally accessible temperature range) where pure fluid behavior of C_{VX} should be observed. This means that the C_{VX}, which diverges

Table V. Values of the Characteristic Parameters for CO_2+ n-Decane Mixtures

x (mole fraction)	K_1	K_2	τ_1	τ_2	$\Delta\bar{\rho}_1$	$\Delta\bar{\rho}_2$
0.095	0.0044	0.023	6.4×10^{-4}	2.09×10^{1}	0.157	4.59×10^{0}
0.178	−0.7050	0.384	2.6×10^{-1}	7.36×10^{2}	1.106	1.46×10^{1}
0.263	−2.9850	1.133	2.1×10^{0}	3.25×10^{6}	2.350	2.23×10^{2}

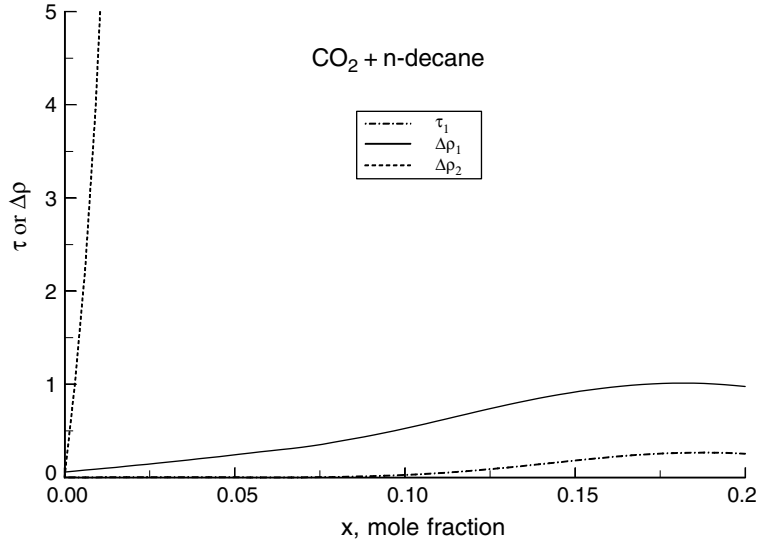

Fig. 10. Characteristic temperature (τ_1) and densities ($\Delta\bar{\rho}_1$, $\Delta\bar{\rho}_2$) as a function of the concentration of n-decane.

weakly for pure CO_2 ($x=0$) with an exponent $\alpha=0.110$, $C_V \propto \tau^{-\alpha}$, will be renormalized by the factor $1/(1-\alpha)(-\alpha \Rightarrow \alpha/(1-\alpha))$, $C_{VX} \propto \tau^{\alpha/(1-\alpha)}$. The isochoric heat-capacity measurements for $CO_2 + n$-decane mixtures ($x=0.095$ and $x=0.178$ mole fraction of n-decane) reported in this work, along the critical isochore, support the Fisher renormalization of the values of the critical exponent for C_{VX} (see Figs. 3 and 11).

Figure 11 shows experimental C_{VX} for the $CO_2 + n$-decane mixture and for the pure components along their respective critical isochores as a function of $\log\tau$. As this figure shows, the slopes of the $\log C_{VX} - \log\tau$ curves for the mixtures are almost zero, while for the pure components the slopes are both very close to the scaling value of 0.110. This means that, upon approach to the critical point ($\tau \to 0$) along the critical isochore, the singular or fluctuation part of the heat capacity C_{VX} for the $CO_2 + n$-decane mixture is zero ($C_{VX} \sim \tau^{\alpha/(1-\alpha)}$). This means that adding a small amount

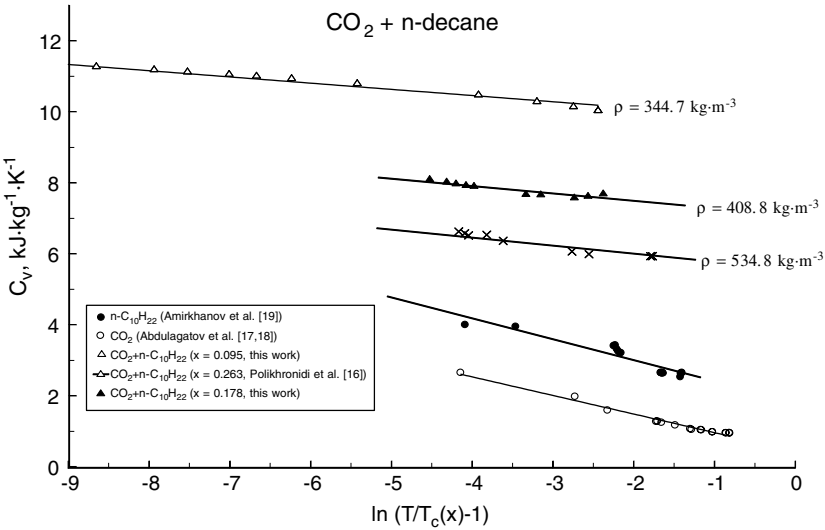

Fig. 11. Isochoric heat capacities C_{VX} of the $CO_2 + n$-decane mixture and their pure components as a function of $\log \tau$ on their critical isochores in the asymptotic regions. Solid lines are guides for the eye.

of n-decane to the critical CO_2 reduce the fluctuation effect on the behavior of the isochoric heat capacity of the mixture. Therefore, the isochoric heat capacity of the $CO_2 + n$-decane mixtures ($x = 0.095$ and $x = 0.178$ mole fraction of n-decane) at the critical point is no longer singular (see Fig. 3). Thus, the behavior of the isochoric heat capacity C_{VX} for these mixtures at the critical points would be completely determined by the regular part (fluctuation-induced background term); C_{VX} for this mixture is constant, at the critical point (see Fig. 3), because C_{VX} exhibits a finite cusp with an infinite slope. The fluctuation-induced, critical contribution (critical enhancement) to $C_{VX}(C_{VX}^{\sin} \cdot \sim \tau^{\alpha/(1-\alpha)} = 0)$ vanishes at the critical point of a mixture ($\tau = 0$). In the pure-component limit ($x \to 0$ or $x \to 1$), the trends of C_{VX} would sharply change to pure-fluid behavior, while for any other composition C_{VX} data exhibit mixture-like behavior (renormalization of the critical exponent). At concentrations above 0.3 mole fraction of n-decane, the slope of the critical $T_C - x$ curve is small (about 100 K). Therefore, the values of the characteristic temperature τ_2 for higher compositions are small (about 5.5×10^{-6}) and experimentally accessible. Perhaps at high concentrations of n-decane, pure-fluid behavior of C_{VX} is possible. Unfortunately, there are no experimental isochoric heat capacity data for compositions above 0.3 mole fraction of n-decane. It is obvious that at the critical temperature extreme, $\frac{dT_C}{dx} = 0$, the isochoric heat capacity of any mixtures behaves just like a pure fluid.

4. SUMMARY

We have measured isochoric heat capacities for $CO_2 + n$-decane mixtures (0.095 and 0.178 mole fraction of n-decane) in a temperature range from 295 to 568 K, at nineteen liquid and vapor densities between 87 and $658\,kg \cdot m^{-3}$ for the composition of 0.095 mole fraction of n-decane and at nine densities between 83 and $458\,kg \cdot m^{-3}$ for the composition of 0.1780 mole fraction of n-decane by using a high-temperature, high-pressure, nearly constant volume adiabatic calorimeter. These ranges include the near-critical and phase-transition regions. The measurements include both the one- and two-phase regions, and the coexistence curve near the critical point. The uncertainties of the C_V and phase transition temperature measurements are estimated to be within 2% (coverage factor $k = 2$) and 0.02 K, respectively. The values of the temperatures and densities at saturation (T_S, ρ_S) and of the critical parameters (T_C, P_C, ρ_C) were extracted from C_V measurements with the quasi-static thermogram technique. The measured values of the critical parameters are in good agreement with values reported in the literature by other authors.

The measured results are used to analyze the critical behavior of the isochoric heat capacity of the $CO_2 + n$-decane mixture in terms of the principle of isomorphism of critical phenomena in binary mixtures. The analysis showed that the experimental isochoric heat capacity data for the $CO_2 + n$-decane mixtures with compositions of 0.095 and 0.178 mole fraction of n-decane support Fisher renormalization of the critical exponent by a factor $1/(1-\alpha)$, as compared to the critical exponent of the pure components. The ranges in the T-x planes for the critical isochore and the ρ-x planes for the critical isotherm, where renormalization of the critical behavior of isochoric heat capacity occurs, were defined. The values of the characteristic parameters (K_1, K_2), temperatures (τ_1, τ_2), and the characteristic density differences ($\Delta\bar{\rho}_1$, $\Delta\bar{\rho}_2$) were estimated by using the critical-curve data and the modern theory of critical phenomena in binary mixtures. The present isochoric heat-capacity measurements are consistent with the behavior predicted by the renormalization theory of critical phenomena in binary mixtures.

ACKNOWLEDGMENT

One of us (I.M.A.) thanks the Physical and Chemical Properties Division at the National Institute of Standards and Technology (NIST) for the opportunity to work as a contractor at NIST during the course of this research. This work was also supported by Grant RFBR 05-08-18229-a.

The authors thank J.W. Magee for his interest in this work and assistance in improving the manuscript and useful discussion.

REFERENCES

1. G. M. Schneider, in *Supercritical Fluids*, E. Kiran and J. M. H. Levelt Sengers, eds. (Kluwer, Dordrecht, 1994), p. 739.
2. G. M. Schneider, in *Proc. Int. Symp. Supercritical Fluids*, M. Perrut, ed. (Nice, France, 1988), p. 1.
3. M. McHugh and V. Krukonis, *Supercritical Fluid Extraction* (Butterworths, London, 1986).
4. *Extraction with Supercritical Gases*, G. M. Schneider, E. Stahl, and G. Wilke, eds. (Verlag Chemie, Weinheim, 1980).
5. S. Saito, *J. Supercritical Fluids* **8**:177 (1995).
6. T. M. Doscher and M. El-Arabi, *Oil Gas J.* **80**:144 (1982).
7. F. M. Orr, M. K. Sliva, and C. L. Lien, *Soc. Pet. Eng. J.* **22**:281 (1982).
8. L. W. Holm, V.A. Josendal, *Soc. Pet. Eng. J.* **22**:87 (1982).
9. F. I. Stalkup, *Soc. Pet. Eng. Monograph* **8** (1983).
10. F. I. Stalkup, *J. Petrol. Tech.* **1**:815 (1983).
11. P. H. van Konynenburg and R. L. Scott, *Phils. Trans. R. Soc. London A* **298**:495 (1980).
12. S. Horstmann, K. Fischer, and J. Gmehling, *J. Chem. Thermodyn.* **32**:451 (2000).
13. G. M. Schneider, *J. Supercritical Fluids* **13**:5 (1998).
14. G. M. Schneider, *Ang. Chem.* **17**:701 (1978).
15. G. M. Schneider, *Fluid Phase Equilib.* **10**:141 (1983).
16. N. G. Polikhronidi, R. G. Batyrova, I. M. Abdulagatov, J. W. Magee, and G. V. Stepanov, *J. Supercritical Fluids* **33**:209 (2004).
17. I. M. Abdulagatov, N. G. Polikhronidi, and R. G. Batyrova, *J. Chem. Thermodyn.* **26**:1031 (1994).
18. I. M. Abdulagatov, N. G. Polikhronidi, and R. G. Batyrova, *Ber. Bunsenges Phys. Chem.* **98**:1068 (1994).
19. Kh. I. Amirkhanov, D. I. Vikhrov, B. G. Alibekov, and V. A. Mirskaya, *Isochoric Heat Capacities and Other Caloric Properties of Hydrocarbons* (DSC Russian Academy of Sciences, Makhachkala, 1981).
20. H. H. Reamer and B. H. Sage, *J. Chem. Eng. Data* **8**:508 (1963).
21. N. Nagarajan and R. L. Robinson, *J. Chem. Eng. Data* **31**:168 (1986).
22. E. S. Gulari, H. Saad, and V. C. Bae, in *Supercritical Fluids. Chemical and Engineering Principles and Applications*, T. G. Squires and M. E. Paulaitis, eds. (ACS Symp. Ser. 329, Washington, DC, 1987), p. 2.
23. N. G. Polikhronidi and R. G. Batyrova, *Russ. High Temperature* **35**:537 (1997).
24. R. D. Shaver, R. L. Robinson, and K. A. M. Gasem, *Fluid Phase Equilib.* **179**:43 (2001).
25. G. F. Chou, R. R. Forbert, and J. M. Prausnitz, *J. Chem. Eng. Data* **35**:26 (1990).
26. B. Bufkin, *M. S. Thesis* (Oklahoma State University, Stillwater, Oklahoma, 1986).
27. G. S. Gurdial, N. R. Foster, S. L. J. Yun, and K. D. Tilly, in *Supercritical Fluid Engineering Sciences*. Fundamentals and Applications (ACS Symposium Ser. 514, Washington, DC, 1993), pp. 34–45.
28. T. Furuya and A. S. Teja, *Ind. Eng. Chem. Res.* **39**:4828 (2000).
29. M. Roth, *Fluid Phase Equilib.* **212**:1 (2003).

30. A. I. Abdulagatov, G. V. Stepanov, and I. M. Abdulagatov, *Russ. J. Structural Chem.* **42**:585 (2001).
31. N. G. Polikhronidi, R. G. Batyrova, and I. M. Abdulagatov, *Fluid Phase Equilib.* **175**:153 (2000).
32. N. G. Polikhronidi, R. G Batyrova, and I. M. Abdulagatov, *Int. J. Thermophys.* **21**:1073 (2000).
33. N. G. Polikhronidi, I. M. Abdulagatov, J. W. Magee, and R. G. Batyrova, *J. Chem. Eng. Data* **46**:1064 (2001).
34. N. G. Polikhronidi, I. M. Abdulagatov, J. W. Magee, and G. V. Stepanov, *Int. J. Thermophys.* **22**:189 (2001).
35. N. G. Polikhronidi, I. M. Abdulagatov, and R. G. Batyrova, *Fluid Phase Equilib.* **201**:269 (2002).
36. N. G. Polikhronidi, I. M. Abdulagatov, J. W. Magee, and G. V. Stepanov, *Int. J. Thermophys.* **23**:745 (2002).
37. N. G. Polikhronidi, I. M. Abdulagatov, J. W. Magee, and G. V. Stepanov, *Int. J. Thermophys.* **24**:405 (2003).
38. B. A. Mursalov, I. M. Abdulagatov, V. I. Dvoryanchikov, A. N. Kamalov, and S. B. Kiselev, *Int. J. Thermophys.* **20**:1497 (1999).
39. N. B. Vargaftik, *Handbook of Physical Properties of Liquids and Gases*, 2nd Ed. (Hemisphere, New York, 1983).
40. W. Wagner and A. Pruß, *J. Phys. Chem. Ref. Data* **31**:387 (2002).
41. F. G. Keyes and L. B. Smith, *Proc. Amer. Acad. Arts Sci.* **68**:505 (1933).
42. I. K. Kamilov, G. V. Stepanov, I. M. Abdulagatov, A. R. Rasulov, and E. I. Milikhina, *J. Chem. Eng. Data* **46**:1556 (2001).
43. V. M. Valyashko, I. M. Abdulagatov, and J. M. H. Levelt-Sengers, *J. Chem. Eng. Data* **45**:1139 (2000).
44. I. M. Abdulagatov, B. A. Mursalov, and V. I. Dvoryanchikov, *J. Chem. Eng. Data* **45**:1133 (2000).
45. J. V. Sengers and J. M. H. Levelt Sengers, in *Progress in Liquid Physics*, C. A. Croxton, ed. (Wiley, New York, 1978), p. 103.
46. J. S. Rowlinson and F. L. Swinton, *Liquids and Liquid Mixtures*, 3rd Ed. (Butterworth Scientific, London, 1982).
47. M. G. Rabezkii, A. R. Bazaev, I. M. Abdulagatov, J. W. Magee, and E. A. Bazaev, *J. Chem. Eng. Data* **46**:1610 (2001).
48. A. R. Bazaev, I. M. Abdulagatov, J. W. Magee, E. A. Bazaev, and A. E. Ramazanova, *Int. J. Thermophys.* **25**:805 (2004).
49. M. A. Urusova and V. M. Valyashko, *Russ. J. Inorg. Chem.* **46**:770 (2001).
50. M. A. Urusova and V. M. Valyashko, *Russ. J. Inorg. Chem.* **46**:777 (2001).
51. N. G. Stretenskaya, R. J. Sadus, and E. U. Franck, *J. Phys. Chem.* **99**:4273 (1995).
52. V. M. Shmonov, R. J. Sadus, and E. U. Franck, *J. Phys. Chem.* **97**:9054 (1993).
53. A. E. Mather, R. J. Sadus, and E. U. Franck, *J. Chem. Thermodyn.* **25**:771 (1993).
54. E. W. Lemmon and R. Span, *J. Chem. Eng. Data* (in press).
55. R. Span and W. Wagner, *J. Phys. Chem. Ref. Data* **25**:1509 (1996).
56. A. I. Abdulagatov, G. V. Stepanov, and I. M. Abdulagatov, submitted to *Russ. J. High Temp*.
57. J. C. Rainwater, *Int. J. Thermophys.* **10**:357 (1989).
58. M. A. Anisimov, *Critical Phenomena in Liquids and Liquid Crystals* (Gordon and Breach, Philadelphia, 1991).
59. M. A. Anisimov, E. E. Gorodezkii, V. D. Kulikov, and J. V. Sengers, *Phys. Rev. E.* **51**:1199 (1995).

60. M. A. Anisimov, E. E. Gorodezkii, V. D. Kulikov, A. A. Povopdyrev, and J. V. Sengers, *Physica A* **220**:277 (1995).
61. M. A. Anisimov and J. V. Sengers, in *Equations of State for Fluids and Fluids Mixtures*, J. V. Sengers, R. F. Kayser, C. J. Peters, and H. J. White, eds. (Elsevier, Amsterdam, 2000), p. 381.
62. M. E. Fisher, *Phys. Rev. B* **176**:257 (1968).
63. Kh. S. Abdulkadirova, A. Wyczalkowska, M. A. Anisimov, and J. V. Sengers, *J. Chem. Phys.* **116**:4597 (2002).
64. P. C. Albright, T. J. Edwards, Z. Y. Chen, and J. V. Sengers, *J. Chem. Phys.* **87**:1717 (1987).
65. I. R. Krichevskii, *Russ. J. Phys. Chem.* **41**:1332 (1967).
66. J. M. H. Levelt Sengers, G. Morrison, G. Nielson, R. F. Chang, and C. M. Everhart, *Int. J. Thermophys.* **7**:231 (1986).
67. J. M. H. Levelt Sengers, in *Supercritical Fluid Technology*. J. F. Ely and T. J. Bruno, eds. (CRC Press, Boca Raton, Florida, 1991), p. 1.